RSC Advances

PAPER

View Article Online
View Journal | View Issue

Cite this: *RSC Adv.*, 2017, **7**, 6303

Highly uniform distribution of Pt nanoparticles on N-doped hollow carbon spheres with enhanced durability for oxygen reduction reaction

Qiurong Shi,[a] Chengzhou Zhu,[a] Mark H. Engelhard,[b] Dan Du[a] and Yuehe Lin*[a]

Received 18th October 2016
Accepted 6th January 2017

DOI: 10.1039/c6ra25391a

www.rsc.org/advances

Carbon-supported Pt nanostructures currently exhibit great potential in polymer electrolyte membrane fuel cells. Nitrogen-doped hollow carbon spheres (NHCSs) with extra low density and high specific surface area are a promising carbon support for loading Pt NPs. The doped heteroatom of nitrogen not only contributes to the active activity for the oxygen reduction reaction (ORR), but also shows a strong interaction with Pt NPs for entrapping them to prevent dissolution/migration. This synergetic effect/interaction resulted in the uniform dispersion and strong combination of the Pt NPs on the carbon support and thus plays a significant role in hindering the degradation of the catalytic activities of Pt NPs. As expected, the as-obtained Pt/NHCSs displayed improved catalytic activity and superior durability toward the ORR.

Introduction

Currently, intensive efforts have been devoted to developing polymer electrolyte membrane fuel cell (PEMFC)-based energy conversion devices for their high power density, facile maintenance, environmental benignity and energy sustainable merits and so on. Therefore, PEMFCs are expected to be widely commercialized for use in transportation, stationary machines and portable electronic devices in the future.[1–4] However, the cathode of PEMFCs employing Pt-based nanoparticles (NPs) dispersed on carbon black (CB) limits the fast development and mass production of PEMFCs-based devices for several critical issues. One problem is that a large amount of Pt loading is required to overcome the sluggish reaction kinetic of oxygen reduction reaction (ORR) to obtain a desirable mass activity (MA).[5–10] Insufficient long-term operation durability is another serious problem that resulted from the serious dissolution, aggregation or Ostwald ripening of Pt-based NPs.[9] One way to tackle the above-mentioned issues is to modify the shapes, morphologies, compositions of Pt-based electrocatalysts to reduce the total cost and enhance the overall catalytic performances.[11–16] Another effective way is by fabrication of efficient carbon support to take advantage of the interaction and synergetic effect between catalysts and support.[17–20]

Because of the large versatility of carbon structures, carbon nanotubes (CNTs), graphene sheet, aerogel or foam, carbon nanofibers, yolk–shell or hollow carbon spheres (HCSs), *etc.* have been chosen as substitutes of carbon black to gain an extended lifetime of PEMFCs.[21–24] HCSs as one kind of novel carbon materials have long been appealing in various energy storage and conversion devices, biomedicine and environmental treatment due to their unique structures with low density, high surface to volume ratio and high mechanical strength.[25–28] HCSs could effectively improve the dispersion of Pt-based electrolytes and stabilize Pt NPs from dissolution and aggregation *via* steric effect generated from pore confinement or encapsulation.[29,30] Besides, introducing heteroatoms like nitrogen into the carbon materials is now very popular in enhancing the electrocatalytic activities, such as nitrogen-doped graphene,[31] CNTs,[32] polyaniline[33] *etc.* They all exhibited enhanced electrochemical performances not only because of the synergetic effect between electrocatalysts and carbon support, but also due to their contribution to electron donor tendency and generation of carbon active sites for arching Pt seed.[34–36]

Here, we reported the *in situ* growth of Pt NPs on N-doped HCSs (NHCSs) with highly uniform distribution and sizes of about 3–5 nm at room temperature, employing formic acid as reducing agent. This reaction happens without any stirring or ultrasonic vibration, indicating a very simple and energy-saving method for mass production of the electrocatalysts. What's important is that the as-obtained Pt NPs are totally surfactant free, which could avoid the tedious work of washing process and is more favorable for direct use as cathode materials for ORR. The as-synthesized Pt NPs decorated NHCSs (Pt/NHCSs) exhibited excellent electrocatalytic performance toward ORR with MA 3.7 times higher than commercial Pt/C at 0.90 V, and half-potential shift of only 9.9 mV after accelerated durability test (ADT), which is much smaller than that of commercial Pt/C. This work demonstrates that Pt/NHCSs are truly promising cathode materials for PEMFCs and the facile synthesis strategy is applicable for a large-scale industrial production.

[a]*School of Mechanical and Material Engineering, Washington State University, Pullman, WA 99164, USA. E-mail: yuehe.lin@wsu.edu*

[b]*Environmental Molecular Sciences Laboratory, Pacific Northwest National Laboratory, Richland, WA 99352, USA*

Experimental

Chemical and materials

Chloroplatinic acid hexahydrate ($H_2PtCl_6 \cdot 6H_2O$), dopamine, tetraethyl orthosilicate (TEOS), ammonia hydroxide ($NH_3 \cdot H_2O$), formic acid, Tris base were all purchased from Sigma-Aldrich Co. Ltd. Ethanol were purchased from Decon Labs, Inc. All magnetic stirring bars and glasswares were cleaned using chloroazotic acid (HCl (37%) : HNO_3 (65%) with 3 : 1 v/v) and then rinsed with deionized (DI) water for at least three times. (**Caution**: chloroazotic acid is very dangerous and shoule be used carefully.) The DI water used in experiments was all acquired from Millipore Milli-Q plus 185 purification system and the resistivity should be higher than 18.2 MΩ cm.

Synthesis of hollow carbon spheres

Silica spheres were firstly synthesized as hard templates by Stöber method.[37] Then, 80 mg of silica spheres were mixed with 80 mg of dopamine in 25 mL of Tris-buffer (0.01 M, pH = 8.5) for 24 h. The polymer/silica nanocomposite was collected *via* centrifugation. Then, carbonization was processed under N_2 atmosphere firstly at 400 °C for 2 h with a heating rate of 1 °C min^{-1}, followed by a second treatment at 800 °C for 3 h with a heating rate of 5 °C min^{-1}. Hollow carbon spheres were collected after washing in sodium hydroxide at 70 °C for 12 h.

Synthesis of Pt/NHCSs

Pt/NHCSs were obtained *via* mixing with $H_2PtCl_6 \cdot 6H_2O$, hollow carbon spheres and formic acid *via* ultrasonic for 15 min, followed by reaction for 48 h without stirring at room temperature, and washed three times with water.[38]

Preparation and electrochemical measurements of electrode

The homogeneous Pt/NHCSs and commercial Pt/C catalyst ink (2 mg mL^{-1}) were prepared *via* dispersing the sample powders into an aqueous solution containing 2 mL 2-propanol, 0.05 mL Nafion (5%) and 8 mL deionized water, respectively, followed by ultrasonic agitation.

The electrochemical experiments were conducted *via* a standard three-electrode electrochemical workstation (CHI 630E). A Pt wire was used as the counter electrode and a $Hg/HgCl_2$ electrode filled with saturated potassium chloride aqueous solution were employed as the reference electrode. The working electrode was prepared with a loading of 25.5 μg cm^{-2} of Pt on a rotating disk electrode (RDE) (0.196 cm^2 in geometric area) and then dried at 60 °C under vacuum. 120 mL 0.1 M $HClO_4$ solution was used as the electrolyte for ORR test.

Cyclic voltammetry (CV) and linear sweep voltammetry (LSV) measurements were performed on RDE connected with an electrode rotator (purchased from Princeton Applied Research). CV tests for ORR were conducted after purging nitrogen or oxygen into 0.1 M $HClO_4$ solution for 30 min. LSV measurements were conducted in O_2-saturated electrolyte.

Characterization

Transmission electron microscopy (TEM) images were acquired by Field Emission Instruments (FEI) (Philips CM200 UT, USA). Energy-dispersive X-ray (EDX) analysis was obtained using FEI sirion field emission scanning electron microscope (FESEM). The tube was operated at 15 mA current and 40 kV accelerating voltage. X-ray Diffraction (XRD) spectrum was obtained from Rigaku Miniflex 600. X-ray photoelectron spectroscopy (XPS) tests were conducted utilizing a Physical Electronics Quantera Scanning X-ray Microprobe. Excitation and a spherical section analyzer were obtained using a focused monochromatic Al Kα X-ray (1486.7 eV) source.

Results and discussion

Polydopamine (PDA)@silica spheres were firstly obtained *via* polymerization of dopamine both as carbon and nitrogen source utilizing silica nanosphere as hard template. After carbonization, NHCSs with diameter of about 200 nm were obtained after removing silica nanospheres by sodium hydroxide. Decoration of uniform Pt NPs was achieved *via* adding H_2PtCl_6 and HCOOH aqueous solution at room temperature and stored for 48 h. Typically, the chemical reaction between H_2PtCl_6 and HCOOH is as follows:

$$H_2PtCl_6 + 2HCOOH \rightarrow Pt + 6Cl^- + 6H^+ + CO_2$$

Fig. 1A–F showed the as-synthesized Pt/NHCSs with different loading ratios from 66.1% (marked as Pt/NHCSs-1), 79.6% (Pt/NHCSs-2) to 88.6% (Pt/NHCSs-3), respectively. The Pt particle size with Pt loading of 66.1% is about 2.8 ± 0.5 nm, while those of 79.6% and 88.1% are about 3.4 nm ± 0.4 nm and 4.8 nm ± 0.6 nm, respectively. From TEM images of these three loading ratios, Pt NPs of Pt/NHCSs-1 appears to be a little bit sparse, while Pt NPs of Pt/NHCSs-3 seems to be too intensive, which may result in a larger particle size caused by the aggregation of NPs. While NHCSs with 79.6% loading shows a moderate size and a more homogeneous distribution on HCS.

The composition of as-fabricated Pt/NHCSs-2 was further confirmed *via* X-ray diffraction (XRD) shown in Fig. 2A. The diffraction peaks were typical face-centered cubic Pt lattice, shown as (111), (200), (211), (311) and (222). The EDX result shown in Fig. 2B also verified the main composition of Pt/NHCSs was Pt. The Pt loading amount of Pt/NHCSs-2 were confirmed *via* thermogravimetric analysis (TGA), shown in Fig. 2C. A total weight loss of about 22.3% were obviously observed after the temperature reached about 800 °C, which was ascribed to the oxidation of NHCSs at 800 °C. The weight loss is almost in agreement with the desired Pt loading of about 79.6% in Pt/NHCSs-2, indicating a complete yield of Pt *via* formic acid reduction method.

We further confirmed the composition of as-synthesized Pt/NHCSs-2 *via* employing XPS. The peak appeared at 400.2 eV and 398.1 eV in Fig. 3A are corresponding to N 1s, which could be further deconvoluted into four peaks including pyridinic N (398.4 eV), pyrrolic N (400.3 eV), graphitic N (401.2 eV) and

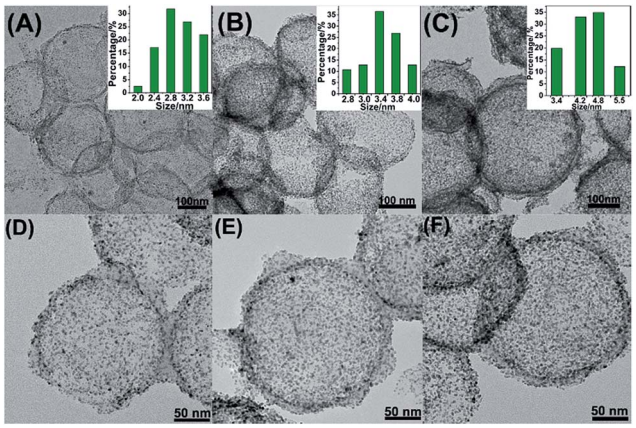

Fig. 1 TEM images of as-synthesized Pt/NHCSs with Pt loading amount of 66.1% (A and D), 79.6% (B and E) and 88.6% (C and F), respectively. The inset pictures in (A–C) are their related size distribution.

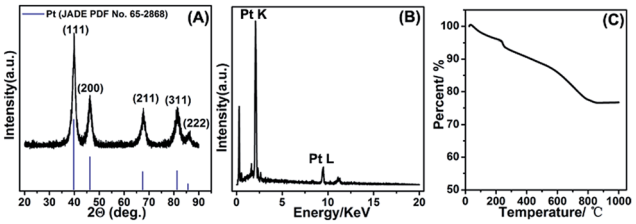

Fig. 2 XRD pattern (A), EDX (B) and TGA curve (C) of as-fabricated Pt/NHCSs-2.

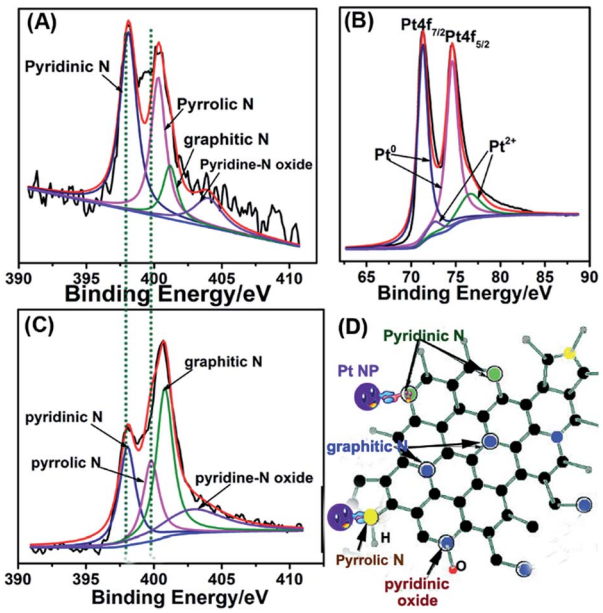

Fig. 3 X-ray photoelectron spectroscopy (XPS) of the N 1s (A), Pt 4f (B) of as-synthesized Pt/NHCSs-2 and N 1s (C) of the as-obtained NHCSs, respectively. (D) Schematic illustration of the four types of nitrogen and their strong interaction with Pt NPs.

pyridine-N oxide (403.9 eV), respectively. The content of these four types of nitrogen is about 44.7%, 31.1%, 11.6% and 12.6%, respectively. The peak of N-HCs in Fig. 3C could be further deconvoluted into four peaks including pyridinic N (398.1 eV), pyrrolic N (399.8 eV), graphitic N (400.8 eV) and pyridine-N oxide (402.9 eV), respectively. The origin content of these four types of nitrogen is about 24.7%, 20.0%, 37.8% and 17.5%, respectively. The N content in N-doped hollow carbon sphere is about 3.44% and that in Pt/NHCSs with Pt loading amount of 79.6% is about 3.84%. It could be seen that the content of pyridinic N and pyrrolic N have been increased and also the binding energy shifted due to the interaction with metal NPs. A first principles study reported that pyrrolic and pyridinic N offered the defect site for the *in situ* nucleation and growth of Pt NPs due to the induced partial charges on neighboring carbon atoms.[32,39] An improved performances toward ORR of mesoporous N-doped carbons containing mainly quaternary N-groups was highlighted as a result of the chemical interaction between Pt NPs and N-defects.[40] Besides, pyridinic and graphitic N acted as active sites for contributing to the ORR performances.[35,41–43] Therefore, it is believed that they could display a catalytic behaviour toward ORR. The N-doped carbon sphere is beneficial in modifying the electronic structure of Pt, leading to the reduced binding energy and adsorption of intermediate on Pt surface[31,43,45] Similarly, the peaks in Fig. 3B appeared at 74.6 eV and 71.3 eV are corresponding to the Pt $4f_{5/2}$ and Pt $4f_{7/2}$, respectively. They also can be deconvoluted into four peaks at 74.6 eV, 71.0 eV and 76.6 eV, 72.4 eV, which are assigned to be metallic state (Pt^0) and oxide state (Pt^{2+}) of Pt, respectively. It is obvious Pt is mainly consists of Pt^0. Besides, the Pt 4f peaks showed a positive shift compared to commercial Pt/C (70.3 eV and 74.0 eV, respectively).[44] The binding energy shift of the N 1s and Pt 4f both indicated a strong interaction between the doped nitrogen atoms and Pt NPs, which would be critical and beneficial in maintaining the long-term catalytic abilities for its unique capability of "entrapping" NPs from aggregation, migration or dissolution.

According to the XPS result, the interaction/synergetic effect between Pt NPs and nitrogen-doped carbon support may play an important role in boosting the electrocatalytic activities and long-term operation stabilities.[46] The electrochemical active surface areas (ECSAs) of the as-fabricated Pt/NHCSs-1, Pt/NHCSs-2, Pt/NHCSs-3 and commercial Pt/C were calculated from the hydrogen adsorption/desorption peak (0.08–0.26 V) in CV curves in N_2-saturated 0.1 M $HClO_4$ aqueous solution, shown in Fig. 4A. The ECSA results of as-obtained Pt/NHCSs were listed in Table 1, which were comparable to commercial Pt/C. From the inset in Fig. 4A, we can see that Pt/NHCSs-2 shows a more positive Pt oxide reduction peak (0.833 V) than commercial Pt/C (0.810 V), indicating a weaker bond connection between Pt surfaces and oxygen containing species, which is favorable for ORR catalytic performances.[47]

Fig. 4B exhibited the LSV curves for ORR utilizing the four kinds of electrocatalysts on a rotating disk electrode (RDE) in O_2-saturated 0.1 M $HClO_4$ solution at a rotating rate of 1600 rpm and a scan rate of 10 mV s^{-1}. The onset potential of the four electrocatalysts was listed in Table 1. It is found that Pt/NHCSs-

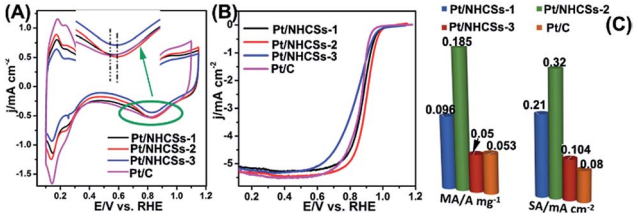

Fig. 4 (A) CV curves of as-obtained Pt/NHCSs-1, Pt/NHCSs-2, Pt/NHCSs-3 and commercial Pt/C in N_2-saturated 0.1 M $HClO_4$ aqueous solution. (B) LSV curves of the four electrocatalysts at a rotation rate of 1600 rpm and a scan rate of 10 mV s^{-1}. (C) MA and SA of the four electrocatalysts at 0.9 V.

2 exhibited a more positive onset potential than the other three samples, implying a more active behavior toward ORR. Half-potential ($E_{1/2}$) is another key indicator for evaluating the activity of the electrocatalysts. From Table 1, Pt/NHCSs-2 displayed a 17.02 mV, 22.0 mV and 16.0 mV positive shift compared with Pt/NHCSs-1, Pt/NHCSs-3 and commercial Pt/C, respectively, which also confirmed it a more active electrocatalysts.

MA and SA are usually employed to precisely evaluate the activity of the Pt-based electrocatalysts toward ORR. MA is obtained from kinetic current density (j_k) *via* the Levich–Koutecky equation shown as follows:

$$\frac{1}{j} = \frac{1}{j_k} + \frac{1}{j_d}$$

where j is the measured current density at a specific potential, j_k is the kinetic current density, and j_d is the diffusion-limiting current density.[48] In Fig. 4C, the MA of Pt/NHCSs-2 reached 0.185 A mg^{-1} at 0.90 V, which is about 1.9, 3.7, and 3.5 times higher than that of Pt/NHCSs-1 (0.096 A mg^{-1}), Pt/NHCSs-3 (0.050 A mg^{-1}) and commercial Pt/C (0.053 A mg^{-1}), respectively. Besides, Pt/NHCSs-2 also showed the highest SA (0.32 mA cm^{-2}) among the four electrocatalysts, which is about 1.53, 3.07, and 4 times higher than the other three samples. It is obvious that Pt/NHCSs-2 shows a superior catalytic activity among the four samples.

The ADT test was conducted in O_2-saturated 0.1 M $HClO_4$ solution at a scan rate of 100 mV s^{-1} with the potential between 0.6 V and 1.1 V for 10 000 cycles. Fig. 5A–D displayed the CV curves and LSV curves of the Pt/NHCSs-2 and commercial Pt/C before and after ADT test, respectively. The ECSA degradation of Pt/NHCSs-2 and commercial Pt/C were about 4.8% and 24.7%, respectively. The $E_{1/2}$ of Pt/NHCSs-2 showed a relatively smaller negative shift of about 9.9 mV compared to that of commercial

Table 1 Electrocatalytic performances of Pt/NHCSs-1, Pt/NHCSs-2, Pt/NHCSs-3 and commercial Pt/C electrocatalysts

	ECSA (m^2 g^{-1})	Onset potential/V	$E_{1/2}$ (V)	MA (A mg^{-1})	SA (mA cm^{-2})
Pt/NHCSs-1	45.9	0.951	0.875	0.096	0.209
Pt/NHCSs-2	57.56	0.963	0.892	0.185	0.320
Pt/NHCSs-3	48.11	0.953	0.870	0.050	0.104
Pt/C	66.70	0.921	0.876	0.053	0.080

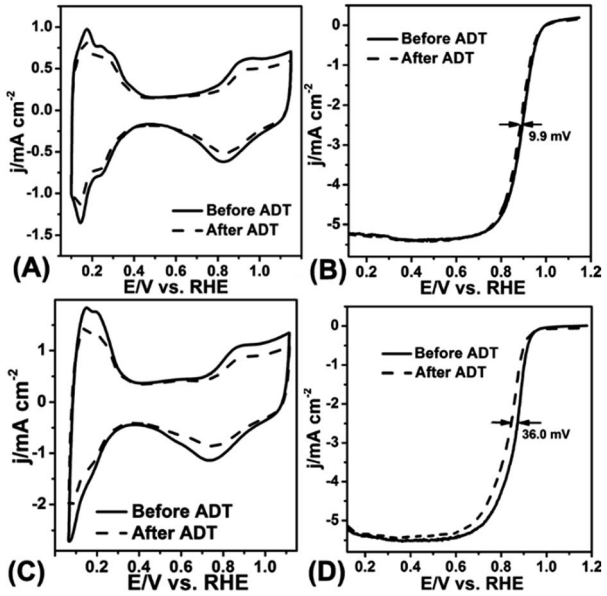

Fig. 5 CV curves of Pt/NHCSs-2 (A) and commercial Pt/C (C) on RDE before and after 10 000 cycles test in N_2-saturated 0.1 M $HClO_4$ solution with a scan rate of 50 mV s^{-1}. LSV curves of Pt/NHCSs-2 (B) and commercial Pt/C (D) on RDE before and after ADT test at a rotation rate of 1600 rpm at a scan rate of 10 mV s^{-1}.

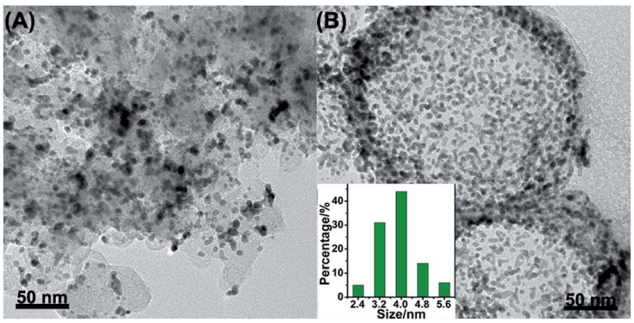

Fig. 6 TEM images of commercial Pt/C (A) and Pt/NHCSs-2 (B) after ADT. The inset in (B) is the size distribution of Pt NPs after ADT.

Pt/C (30.0 mV), indicating an excellent long-term operation durability. Fig. 6A and B exhibited the TEM images of commercial Pt/C and Pt/NHCSs-2 after 10 000 cycle test, respectively. It can be observed that Pt NPs of commercial Pt/C suffered from serious aggregation after ADT, resulting in a poor stability toward ORR, while the morphologies of Pt/NHCSs-2 could be well maintained with the size only changed about 0.6 nm after 10 000 cycle test. It is believed that the strong interaction between the nitrogen sites and Pt NPs plays a significant role in confining Pt NPs from dissolution and aggregation for avoiding the loss of activity.[40,42,47]

Conclusions

In summary, we have synthesized NHCSs with Pt NPs loading *via* a facile and green method applied for ORR. The HCSs as carbon support have the advantage of low density and high

specific density. What's more important is the heteroatom doping hold the key for improving the overall catalytic performance toward ORR: (I) nitrogen doping could help the *in situ* deposition of Pt ions for growth without decorating any other functional groups; (II) the synergetic effect between nitrogen sites and Pt NPs, and pyridinic and graphitic N acting as active sites are critical in enhancing the catalytic activities; (III) the strong interaction between nitrogen sites and Pt catalysts is of great importance in obtaining the long-term operation durability for ORR *via* preventing the Pt NPs from dissolution or aggregation. Overall, the optimized Pt/NHCSs is promising for mass production in application in PEMFCs.

Acknowledgements

This work was sponsored by Washington State University start-up fund. We thank Franceschi Microscopy & Image Center at Washington State University for TEM and SEM measurement. We also thank EMSL, a national scientific user facility for XPS measurement, which is sponsored by the Department of Energy's Office of Biological and Environmental Research located at Pacific Northwest National Laboratory. Q. S. thanks the China Scholarship Council for the financial support.

Notes and references

1 N. Tian, Z. Y. Zhou, S. G. Sun, Y. Ding and Z. L. Wang, *Science*, 2007, **316**, 732–735.
2 B. Lim, M. J. Jiang, P. H. C. Camargo, E. C. Cho, J. Tao, X. M. Lu, Y. M. Zhu and Y. N. Xia, *Science*, 2009, **324**, 1302–1305.
3 M. Winter and R. J. Brodd, *Chem. Rev.*, 2004, **104**, 4245–4269.
4 M. S. Dresselhaus and I. L. Thomas, *Nature*, 2001, **414**, 332–337.
5 H. A. Gasteiger and N. M. Markovic, *Science*, 2009, **324**, 48–49.
6 H. A. Gasteiger, S. S. Kocha, B. Sompalli and F. T. Wagner, *Appl. Catal., B*, 2005, **56**, 9–35.
7 C. Z. Zhu, H. Li, S. F. Fu, D. Du and Y. H. Lin, *Chem. Soc. Rev.*, 2016, **45**, 517–531.
8 C. Z. Zhu, D. Du, A. Eychmuller and Y. H. Lin, *Chem. Rev.*, 2015, **115**, 8896–8943.
9 Y. Y. Shao, J. Liu, Y. Wang and Y. H. Lin, *J. Mater. Chem.*, 2009, **19**, 46–59.
10 S. Zhang, Y. Y. Shao, G. P. Yin and Y. H. Lin, *J. Mater. Chem. A*, 2013, **1**, 4631–4641.
11 S. J. Guo, S. Zhang and S. H. Sun, *Angew. Chem., Int. Ed.*, 2013, **52**, 8526–8544.
12 B. Y. Xia, H. B. Wu, Y. Yan, X. W. Lou and X. Wang, *J. Am. Chem. Soc.*, 2013, **135**, 9480–9485.
13 X. H. Sun, K. Z. Jiang, N. Zhang, S. J. Guo and X. Q. Huang, *ACS Nano*, 2015, **9**, 7634–7640.
14 L. Z. Bu, J. B. Ding, S. J. Guo, X. Zhang, D. Su, X. Zhu, J. L. Yao, J. Guo, G. Lu and X. Q. Huang, *Adv. Mater.*, 2015, **27**, 7204–7212.
15 C. Chen, Y. J. Kang, Z. Y. Huo, Z. W. Zhu, W. Y. Huang, H. L. L. Xin, J. D. Snyder, D. G. Li, J. A. Herron, M. Mavrikakis, M. F. Chi, K. L. More, Y. D. Li, N. M. Markovic, G. A. Somorjai, P. D. Yang and V. R. Stamenkovic, *Science*, 2014, **343**, 1339–1343.
16 X. Q. Huang, Z. P. Zhao, L. Cao, Y. Chen, E. B. Zhu, Z. Y. Lin, M. F. Li, A. M. Yan, A. Zettl, Y. M. Wang, X. F. Duan, T. Mueller and Y. Huang, *Science*, 2015, **348**, 1230–1234.
17 S. J. Guo and S. H. Sun, *J. Am. Chem. Soc.*, 2012, **134**, 2492–2495.
18 W. T. Yu, M. D. Porosoff and J. G. G. Chen, *Chem. Rev.*, 2012, **112**, 5780–5817.
19 X. Q. Huang, Z. P. Zhao, Y. Chen, E. B. Zhu, M. F. Li, X. F. Duan and Y. Huang, *Energy Environ. Sci.*, 2014, **7**, 2957–2962.
20 S. H. Sun, F. Jaouen and J. P. Dodelet, *Adv. Mater.*, 2008, **20**, 3900–3904.
21 R. Kou, Y. Y. Shao, D. H. Wang, M. H. Engelhard, J. H. Kwak, J. Wang, V. V. Viswanathan, C. M. Wang, Y. H. Lin, Y. Wang, I. A. Aksay and J. Liu, *Electrochem. Commun.*, 2009, **11**, 954–957.
22 H. J. Qiu, X. C. Dong, B. Sana, T. Peng, D. Paramelle, P. Chen and S. Lim, *ACS Appl. Mater. Interfaces*, 2013, **5**, 782–787.
23 J. L. Zhu, G. Q. He, Z. Q. Tian, L. Z. Liang and P. K. Shen, *Electrochim. Acta*, 2016, **194**, 276–282.
24 S. Takenaka, H. Miyamoto, Y. Utsunomiya, H. Matsune and M. Kishida, *J. Phys. Chem. C*, 2014, **118**, 774–783.
25 F. Bottger-Hiller, P. Kempe, G. Cox, A. Panchenko, N. Janssen, A. Petzold, T. Thurn-Albrecht, L. Borchardt, M. Rose, S. Kaskel, C. Georgi, H. Lang and S. Spange, *Angew. Chem., Int. Ed.*, 2013, **52**, 6088–6091.
26 Y. H. Ng, S. Ikeda, T. Harada, S. Higashida, T. Sakata, H. Mori and M. Matsumura, *Adv. Mater.*, 2007, **19**, 597–601.
27 Z. C. Yang, Y. Zhang, J. H. Kong, S. Y. Wong, X. Li and J. Wang, *Chem. Mater.*, 2013, **25**, 704–710.
28 J. A. Zhang, K. X. Wang, S. J. Guo, S. P. Wang, Z. Q. Liang, Z. M. Chen, J. W. Fu and Q. Xu, *ACS Appl. Mater. Interfaces*, 2014, **6**, 2192–2198.
29 C. Galeano, J. C. Meier, V. Peinecke, H. Bongard, I. Katsounaros, A. A. Topalov, A. H. Lu, K. J. J. Mayrhofer and F. Schuth, *J. Am. Chem. Soc.*, 2012, **134**, 20457–20465.
30 C. Yang, M. Zhou and Q. Xu, *Nanoscale*, 2014, **6**, 11863–11870.
31 J. B. Zhu, M. L. Xiao, X. Zhao, K. Li, C. P. Liu and W. Xing, *Chem. Commun.*, 2014, **50**, 12201–12203.
32 D. C. Higgins, D. Meza and Z. W. Chen, *J. Phys. Chem. C*, 2010, **114**, 21982–21988.
33 J. Melke, B. Peter, A. Habereder, J. Ziegler, C. Fasel, A. Nefedov, H. Sezen, C. WÖll, H. Ehrenberg and C. Roth, *ACS Appl. Mater. Interfaces*, 2016, **8**, 82–90.
34 L. L. Zhang and X. S. Zhao, *Chem. Soc. Rev.*, 2009, **38**, 2520–2531.
35 K. P. Gong, F. Du, Z. H. Xia, M. Durstock and L. M. Dai, *Science*, 2009, **323**, 760–764.
36 T. Ikeda, M. Boero, S. F. Huang, K. Terakura, M. Oshima and J. Ozaki, *J. Phys. Chem. C*, 2008, **112**, 14706–14709.
37 A. F. Wener Stöber, *J. Colloid Interface Sci.*, 1968, 62–69.
38 A. Postma, Y. Yan, Y. Wang, A. N. Zelikin, E. Tjipto and F. Caruso, *Chem. Mater.*, 2009, **21**, 3042–3044.

39 T. Holme, Y. Zhou, R. Pasquarelli and R. O'Hayre, *Phys. Chem. Chem. Phys.*, 2010, **12**, 9461–9468.
40 L. Perini, C. Durante, M. Favaro, V. Perazzolo, S. Agnoli, O. Schneider, G. Granozzi and A. Gennaro, *ACS Appl. Mater. Interfaces*, 2015, **7**, 1170–1179.
41 L. T. Qu, Y. Liu, J. B. Baek and L. M. Dai, *ACS Nano*, 2010, **4**, 1321–1326.
42 S. B. Yang, X. L. Feng, X. C. Wang and K. Mullen, *Angew. Chem., Int. Ed.*, 2011, **50**, 5339–5343.
43 Y. J. Zhang, K. Fugane, T. Mori, L. Niu and J. H. Ye, *J. Mater. Chem.*, 2012, **22**, 6575–6580.
44 X. Zhao, J. B. Zhu, L. Liang, J. H. Liao, C. P. Liu and W. Xing, *J. Mater. Chem.*, 2012, **22**, 19718–19725.
45 N. Dimakis, N. E. Navarro, T. Mion and E. S. Smotkin, *J. Phys. Chem. C*, 2014, **118**, 11711–11722.
46 S. Zhang, Y. Y. Shao, G. P. Yin and Y. H. Lin, *J. Mater. Chem.*, 2009, **19**, 9289.
47 V. R. Stamenkovic, B. Fowler, B. S. Mun, G. F. Wang, P. N. Ross, C. A. Lucas and N. M. Markovic, *Science*, 2007, **315**, 493–497.
48 M. G. Del Popolo, E. P. M. Leiva, M. Mariscal and W. Schmickler, *Surf. Sci.*, 2005, **597**, 133–155.